International Journal of Applied Earth Observation and Geoinformation 13 (2011) 70–80

Contents lists available at ScienceDirect

International Journal of Applied Earth Observation and Geoinformation

journal homepage: www.elsevier.com/locate/jag

Burnt area delineation from a uni-temporal perspective based on Landsat TM imagery classification using Support Vector Machines

George P. Petropoulos[a,b,*], Charalambos Kontoes[a], Iphigenia Keramitsoglou[a]

[a] Institute of Space Applications and Remote Sensing, National Observatory of Athens, I. Metaxa and Vas. Pavlou St, Penteli, Athens 15236, Greece
[b] INFOCOSMOS, Pindou 71, 13341, Athens Greece

ARTICLE INFO

Article history:
Received 8 February 2010
Accepted 22 June 2010

Keywords:
Burnt area mapping
Landsat TM
Support Vector Machines
Risk-EOS
Greek fires 2007
Remote sensing

ABSTRACT

Information on burnt area is of critical importance in many applications as for example in assessing the disturbance of natural ecosystems due to a fire or in proving important information to policy makers on the land cover changes for establishing restoration policies of fire-affected regions. Such information is commonly obtained through remote sensing image thematic classification and a wide range of classifiers have been suggested for this purpose. The objective of the present study has been to investigate the use of Support Vector Machines (SVMs) classifier combined with multispectral Landsat TM image for obtaining burnt area mapping. As a case study a typical Mediterranean landscape in Greece was used, in which occurred one of the most devastating fires during the summer of 2007. Accuracy assessment was based on the classification overall statistical accuracy results and also on comparisons of the derived burnt area estimates versus validated estimates from the Risk-EOS Burnt Scar Mapping service. Results from the implementation of the SVM using diverse kernel functions showed an average overall classification accuracy of 95.87% and a mean kappa coefficient of 0.948, with the burnt area class always clearly separable from all the other classes used in the classification scheme. Total burnt area estimate computed from the SVM was also in close agreement with that from Risk-EOS (mean difference of less than 1%). Analysis also indicated that, at least for the studied here fire, the inclusion of the two middle infrared spectral bands TM5 and TM7 of TM sensor as well as the selection of the kernel function in SVM implementation have a negligible effect in both the overall classification performance and in the delineation of total burnt area. Overall, results exemplified the appropriateness of the spatial and spectral resolution of the Landsat TM imagery combined with the SVM in obtaining rapid and cost-effective post-fire analysis. This is of considerable scientific and practical value, given the present open access to the archived and new observations from this satellite radiometer globally.

1. Introduction

Forest fires are regarded as one of the most threatening sources of disturbance for property, infrastructure as well as ecosystems. In the Mediterranean region, for millennia fire has been a major ecological factor with a long and important presence (Naveh, 1975; Mayor et al., 2007). The prolonged arid and hot summer periods favour the ignition and rapid propagation of fires especially with strong winds, resulting in large burnt areas every year (Cuomo et al., 2001; FAO, 2001). Nearly 90% of all the wildland forest fires in the European Union take place in the Mediterranean countries (Rosa et al., 2008). Particularly in the last decades, forest fires in the Mediterranean have increased in frequency, as a result of various climatic and anthropogenic factors (Maselli et al., 2003; ECFFE, 2006—Fig. 1).

Being able to obtain accurate as well as rapid mapping of burnt areas after a fire suppression, is of key importance in policy decision making, as it can be used effectively in establishing rehabilitation and restoration policies in the affected areas and also in assisting to avoid post-fire hazards and long-term degradation (Giglio et al., 2006). Burnt area delineation on an operational basis can also provide important information on land cover changes related to ecology and biodiversity, assisting significantly in understanding post-fire recovery of an affected area (Rong et al., 2004). Last but not least, estimates of total area burnt is also a key input parameter in the modelling the atmospheric and climatic impacts of biomass burning, as well as in the estimation of the total atmospheric emissions from it (Kasischke and French, 1995).

* Corresponding author at: Institute for Space Applications and Remote Sensing, National Observatory of Athens, I. Metaxa and Vas. Pavlou St, Penteli, Athens 15236, Greece. Tel.: +30 210 2486905; fax: +30 210 2486905.
E-mail addresses: gpetropoulos@space.noa.gr, petropoulos.george@gmail.com (G.P. Petropoulos), kontoes@space.noa.gr (C. Kontoes), ik@space.noa.gr (I. Keramitsoglou).
URL: http://www.infocosmos.eu (G.P. Petropoulos).

0303-2434/$ – see front matter © 2010 Elsevier B.V. All rights reserved.
doi:10.1016/j.jag.2010.06.008

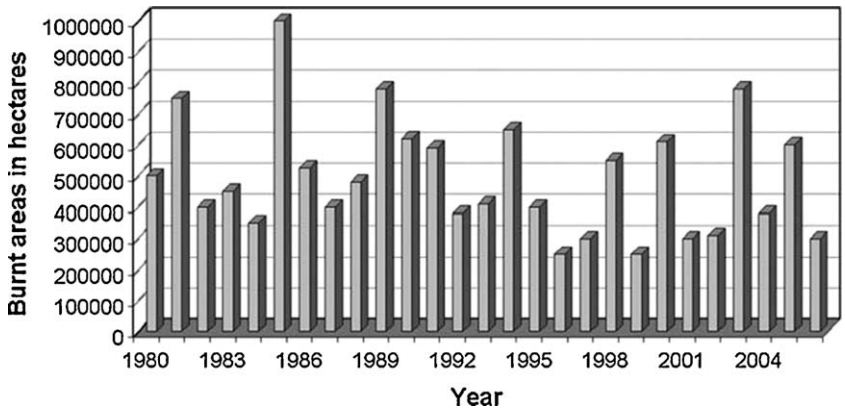

Fig. 1. Yearly reported burnt area at five southern European member states namely: Greece, Italy, Portugal, Spain and France. Adopted from (EU, 2006).

The contribution of remote sensing in fire analysis, including the evaluation of impacts from wildfires was early recognized (Jayaweera and Ahlnas, 1974). Among the advantages of remote sensing compared to conventional field surveys is the provision of timely and often inexpensive imagery at an adequate spatial resolution at low or no cost from local, to regional and global scale. In general, remote sensing methods employed in burnt area mapping have been based on the alteration of the spectral characteristics of the land surface after a fire, which results to a strong contrast between the fire-affected areas and the surrounding environment. These changes are most obvious in the reflective part (0.45–3.0 μm) of the electromagnetic spectrum. Burnt area detection methods are generally categorised according to either the number of satellite observations used in the analysis or the method of image processing carried out. Comprehensive reviews on the topic are available for example in Lentile et al. (2006) and Smith et al. (2007). Briefly, as regards the number of images used, the methods can be uni-temporal or multi-temporal, depending on whether a single post-fire imagery or a pre-fire and post-fire imagery is used. Uni-temporal, also known as single-image, approaches have important advantages over multi-temporal methods, namely their lower cost and shorter processing time (Koutsias et al., 1999). In addition, these methods do not either require precise image-to-image registration or corrections for errors resulting from sun-sensor geometry, atmospheric effects and possibly differences in sensor calibration (Verbyla and Boles, 2000). However, in these approaches, the single-image has to be acquired very shortly after the suppression of the fire as otherwise, the spectral signal of the burnt areas becomes less evident (Corona et al., 2008). What is more, a potential limitation of single-date burned area mapping is that it in such methods is not possible to determine which land cover types have been affected by the fire to assess the post-fire damage if a land cover map of the affected site is not already available for the studied site. On the other hand, multi-temporal approaches offer the advantage of reduced the spectral confusion with the types of permanent cover (Escuin et al., 2008). As far as image processing is concerned, the methods vary from the calculation of simple radiometric indices, such as the Normalised Difference Vegetation Index (NDVI; Deering et al., 1975) and the Normalised Burnt Ratio (NBR; Kasischke and French, 1995), to other more complex approaches such as image classification and sub-pixel analysis methods with pixel spectral unmixing (Kokaly et al., 2007; Eckmann et al., 2008). In addition, there exist the decision tree classification approaches (Simard et al., 2000; Kontoes et al., 2009). A few studies have also proposed the retrieval of burnt area based on surface temperature distribution analysis using the thermal infrared part of electromagnetic spectrum (Eva and Lambin, 2000).

A wide variety of remote sensing sensors are used to delineate burnt area, with Landsat Thematic Mapper (TM) being one of them. This satellite radiometer has a number of advantages for deriving burnt area estimates. It is currently the only high spatial resolution sensor (30 m in the reflective shortwave channels and 120 m in one thermal infrared channel), providing today at no cost – subject to proposal approval in some occasions – global image data at high spectral resolution (7 bands from visible to thermal infrared), compared to freely distributed coarser spatial resolution imagery (e.g. Moderate Resolution Imaging Spectroradiometer – MODIS, Medium Resolution Imaging Spectrometer – MERIS, Advanced Very High Resolution radiometer – AVHRR) or other high spatial resolution radiometers (e.g. Advanced Spaceborne Thermal Emission and Reflection Radiometer – ASTER, Advanced Land Observation Satellite – ALOS) which have on occasion high acquisition cost.

Several studies applying a variety of approaches have addressed the use of Landsat TM in burnt area mapping at various geographical regions (Dixon and Candade, 2008) including the Mediterranean region (Quintano et al., 2006). Many of these studies have been based on the implementation of image classification approaches, demonstrating the usefulness of different classification approaches for burnt area mapping (Sunar and Ozkan, 2001; Kokaly et al., 2007). However, little attention seems to have been paid so far in exploiting the advantages of Support Vector Machines (SVMs, Vapnik, 1995) classifier combined with Landsat TM observations for this purpose. SVMs have several advantages in comparison to other classifiers, as they can be applied requiring limited effort in their training and they do not make any assumption for the probability distribution of the training datasets used as for example is the case for the maximum likelihood parametric classifier. Moreover they are able to deal easily with high dimensionality datasets and have proven to address effectively the ill-posted problems providing high classification accuracies. SVM classifier has generally been implemented in many classification problems using different classes number employed in classification and remote sensing data acquired at different spatial scales (e.g. SPOT, MODIS, Landsat TM/ETM+) producing reliable results (e.g. Huang et al., 2008; Carrao et al., 2008; Knorn et al., 2009; Kavzoglu and Colkesen, 2009). Other investigators have also examined the potential use of SVM classifier combined with hyperspectral data, reporting also generally good results (Pal, 2006; Dalponte et al., 2009). Nevertheless, to our knowledge, very few research studies have so far investigated the potential importance of kernel function selection in the success of the SVM classification (e.g. Keuchel et al., 2003; Li and Liu, 2010). Also, very few works have been directed so far in examining the effect of spectral bands information inclusion to the SVM classification performance, and this has been done only for limited types of kernel functions (e.g. Huang et al., 2002; Zammit et al., 2006; Cao et

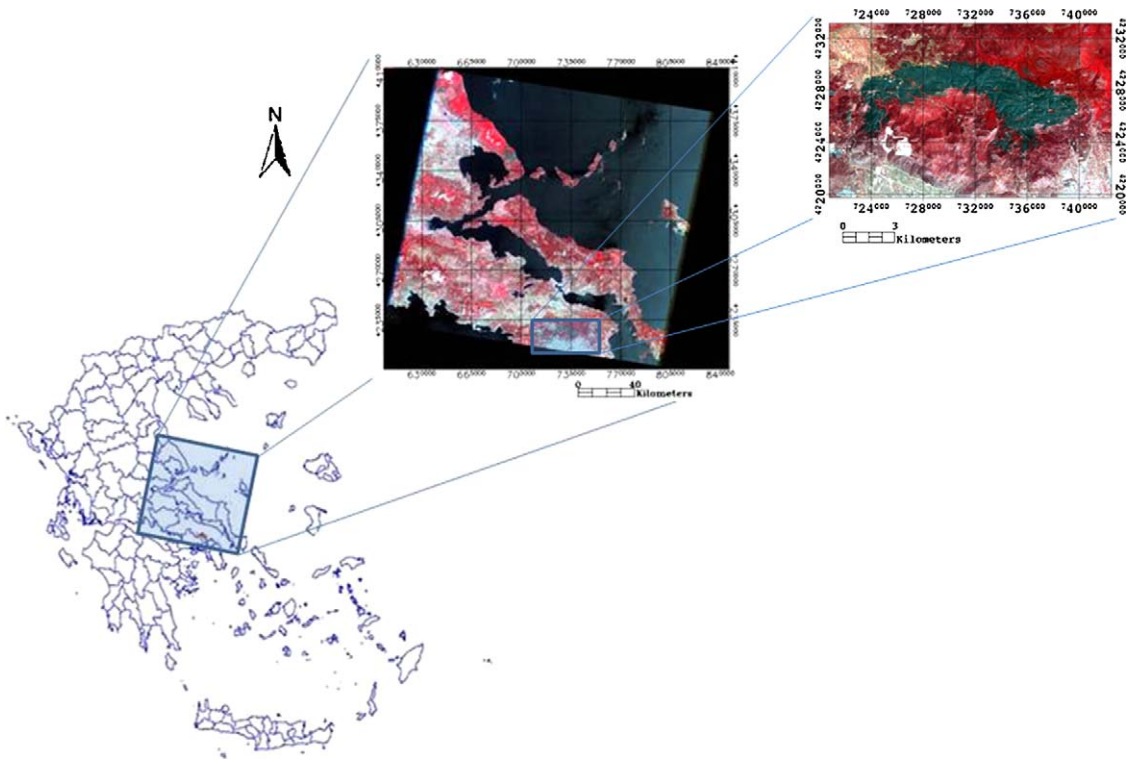

Fig. 2. Location of the study site is shown on the left side of the map. On the centre is illustrated the Landsat-5 TM satellite imagery acquired for the site on July 3rd, 2007, just a few days after the fire suppression. Study site shown in the subset of the Landsat TM post-fire imagery with acquisition date on July 3rd, 2007. With the black color is depicted the burn scar.

al., 2009). What is more, the potential added value of SVM classifier with remote sensing data for burnt area mapping has also not adequately investigated as yet; studies implemented so far have only been based on binary classification approach (burnt/non-burnt), thus not fully exploiting the SVM potential to use the quantity of spectral information from the remote sensing imagery for separating the burnt area from the other land surface classes (Zammit et al., 2006; Cao et al., 2009). Furthermore, the question remains today on whether SVM combined particularly with the spectral quality and high spatial accuracy of Landsat TM imagery is sufficient to provide a cost-effective means to rapidly map burnt scars and assess post-fire damage.

The present study addresses the above questions and has a main objective to explore for the first time the potential value of the combined use of the SVM with Landsat TM observations for accurate and cost-effective burnt area cartography in a Mediterranean setting. In this framework, this study also investigates the effect of kernel function selection and of different Landsat TM spectral bands input to the overall classification accuracy, but also in the delineation of the burnt area class in particular. Furthermore, the present work also builds on previous studies concerned with the evaluation of mapping the burnt area extent at national level, a topic of sustained interest until today (Bochetti et al., 2008; Kontoes et al., 2009; Petropoulos et al., 2010).

2. Experimental set-up

2.1. Study site

The study site comprises the wider area of Mt. Parnitha, located about 30 km north of Athens, Greece (Fig. 1). The study area covers approximately 200 km^2 with an altitude ranging from 200 to 1400 m above sea level and slopes ranging from 3 to 90%. Mt. Parnitha is representative of the mixed characteristics of the eastern Mediterranean regions covered by Greek Fir and Aleppo Pine forest at altitudes between 300 and 1000 m. Above 1000 m height the dominant land types are grassland and scrubland, and below 300 m farmland (to the north) and suburban housing (to the east). The region of Mt. Parnitha is also included in the European network of protected areas Natura 2000 due to the presence of its high biodiversity. Mt. Parnitha experienced severe damage from a wildfire outbreak on June 28th, 2007, which was suppressed five days later (July 1st, 2007).

2.2. Datasets description

A Landsat-5 TM multispectral imagery (path: 183, row: 33) with an acquisition date of July 3rd, 2007 – 2 days after the fire suppression – was obtained at no cost from the United Stated Geological Survey (USGS) archive (http://glovis.usgs.gov/) (Fig. 2). Image selection was based on the fulfillment of criteria of cloud-free conditions and acquisition date as close as possible to the fire event. In addition to the TM imagery, the CORINE 2000 Land Cover (CLC) map (JRC-EEA, 2005) at a spatial resolution of 100 meters for the site was obtained at no cost (from http://reports.eea.europa.eu/COR0-landcover/en). Furthermore, the burnt area map from the Risk-EOS Burnt Scar Mapping service for this specific fire event was obtained. Risk-EOS (http://www.risk-eos.com/actus/pge/index.php?arbo=0) was developed in the framework of the GMES-SE programme (Global Monitoring for Environmental Security/Service Element) of the European Space Agency. It is an operational and validated crisis response service to situations engendered by natural disasters, covering from prevention to crisis management and damage assessment. Benchmarking studies performed recently concerning the evaluation of burnt area estimates computed based on the Risk-EOS methodology have indicated a burnt area detection capability over scars size of the order of 0.1 ha (Kontoes et al., 2009) using high resolution satellite imagery. For this specific fire event at Mt.

Parnitha, the Risk-EOS service burnt area estimate had been based on the application of a fixed thresholding method applied to a post-fire SPOT (XS) imagery (20 m spatial resolution). The derived burnt area map was subsequently validated and fine-tuned by visual photo-interpretation and on-screen digitization of an orthorectified very high spatial resolution satellite imagery (IKONOS) assisted also by on-site conducted GPS measurements (Kontoes et al., 2009).

3. Support Vector Machines

In this section a summary of the principles of SVM classification method is provided, whereas comprehensive description of method operation can be found for example in Burges (1998) and Foody and Mathur (2004). SVM is a supervised machine learning method preforming supervised classification based on statistical learning theory (Vapnik, 1995).

To full understand the SVM operation, let us assume first the simplest scenario of a binary classification, where two classes needed to be linearly separated. First, we assume that a set of representative training data has been collected, which will be used to perform the binary classification. On this basis, the training set is represented as a feature vector $\vec{x_1}, \ldots, \vec{x_N}$, and the corresponding training labels which have also previously defined are represented as $y_1, \ldots, y_N$, where $y_i \in [-1, +1]$, as here we consider the binary case.

In its simplest form, the linear SVM attempts to calculate the hyperplane $\vec{w}$, defined as $\vec{w} = w_1, \ldots, w_N$ which is able to best separate the positive (i.e. +1) from the negative training points selected (i.e. −1). From all possible hyperplanes that can separate the training examples, it is chosen the one that maximises the sum of the distance defined between the hyperplane and the nearest positive and negative training example, called the margin, and this hyperplane is called "optimal hyperplane". For the case where the margin is parameterized as a linear hyperplane with an offset b, the latter is expressed as:

$$\vec{w} \cdot \vec{x} + b = 0 \quad (1)$$

where in the above equation x is a point lying on the hyperplane, w is a parameter determining the hyperplane orientation in space, and b represents the distance of the hyperplane from the origin. Each of data points must fall on the proper side of the hyperplane, as follows:

$$y_i \cdot \vec{x_i} + b \geq +1 \quad (2)$$

$$y_i \cdot \vec{x_i} + b \leq +1 \quad (3)$$

where the above two equations, combined are expressed from the following inequality:

$$y_i(\vec{x_i} \cdot \vec{w} + b) - 1 \geq 0, \quad (4)$$

From all the training data points, those which are parallel to the optimum hyperplane are called support vectors, and are essentially the points which satisfy the equation:

$$y_i(\vec{x_i} \cdot \vec{w} + b) - = \pm 1 \quad (5)$$

Thus, the otpimal hyperplane can be found by minimizing $\vec{w}$ while satisfying Eq. (4) from which it shown that this is happening when the margin is be equal to $2/||\vec{w}||$.

In order to represent more complex hyperplane shapes than linear, the techniques can be extended using kernel functions, $K(\vec{x}_i, \vec{w})$ replacing the vector product in Eqs. (1) and (4). In this case, the problem transforms into an equivalent linear hyperplane problem of higher dimensionality. Use of the kernel function essentially allows the data points to be classified to spread in a way that allows the fitting of a linear hyperplane. SVM also introduces a cost parameter C to quantify the penalty of misclassification errors in order to handle non-separable classification problems. Commonly used SVM kernels include the polynomial, the radial basis function (RBF) and the sigmoid kernels, whereas new kernels can also be obtained from simple mathematical operations of kernels.

4. Methodology

4.1. Landsat TM pre-processing

The Landsat-5 TM Level 1T image obtained from USGS archive is precision and terrain-corrected. The geo-referencing accuracy of the image was initially checked versus a reference IKONOS imagery (equivalent scale map 1:10,000) of the same area, available from a previous study. Comparison indicated a positional error in the order of the pixel size of the TM image (i.e. 30 m), that was considered adequate for the purposes of this study. All image processing that followed was subsequently applied to this specific TM imagery and was performed in ENVI software (v4.7, ITT Visual Information Solutions). ENVI is a commercial image processing platform dedicated to digital imagery visualisation and analysis which includes advanced image processing and analysis tools for a wide variety of remote sensing data. In order to achieve faster computational processing, the first step involved performing a subset from the acquired imagery of the wider area covering the region of Mt. Parnitha (Fig. 2, right). The next step involved the selection of the number of classes as well as of the TM spectral bands to be used for the SVM implementation. The classification scheme used herein included five classes, namely: burnt area, agricultural areas, forests, scrubland/herbaceous vegetation, and urban fabric/bare soil areas. Regarding the number of spectral bands used in the SVM-based classification, initially the first four (TM1, TM2, TM3 and TM4) and subsequently all the six optical bands of TM sensor were used to define the multi-dimensional feature space of the SVM classifier. This was decided in order to gain an insight into the sensitivity of the overall SVM results to the spectral bands combination used as input in its parameterization stage.

The next step involved the selection of the training and validation set of pixels from the TM imagery for the SVM implementation and validation of the produced thematic maps, respectively. Generally, it is suggested that a minimum of 10–30p cases per class be used for training, where p is the number of wavebands used (Piper, 1992; Mather, 2004; Van Niel et al., 2005). In addition, specifically for SVM, previous studies have shown that this classifier is able to generally provide very satisfactory classification results when small training sets are used (Pal and Mather, 2006). In our study approximately 180 representative training pixels for each class were selected from the Landsat TM image based on a random distribution. An additional set of approximately 60 pixels for each class, also randomly selected, was also selected with the intention to be used in the validation of the produced thematic maps. Selection of the most spectrally pure pixels for each class was mainly based on the CLC2000 map of the studied region obtained previously validated where necessary on the IKONOS imagery which was also available for the studied region as mentioned before. As a further test of the appropriateness of the selected training and validation sets pixels for each class, it was computed their statistical separability in ENVI using both the Jeffries–Matusita and the Transformed Divergence separability statistical measures (ENVE User's Guide, 2008). This software feature allows computing the spectral separability of collected regions of interest, with reference to a number of spectral channels of an input file (multispectral or hyperspectral satellite imagery) considered each time. Generally, spectral separability values ranges from 0 to 2.0 and indicate how well the selected regions of interest spectral pairs are statistically separate. Values greater than 1.9 generally are interpreted as

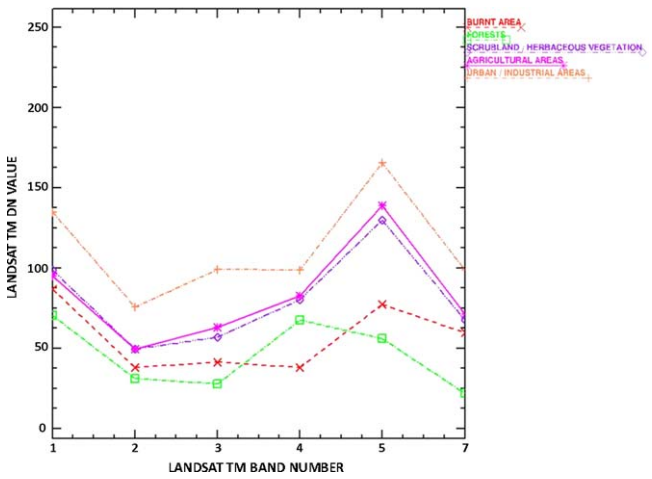

Fig. 3. Average spectral signatures of the selected training sites for all the classes used in the SVM classifier implementation with Landsat TM imagery. DN refers to the pixels' digital number. The central wavelengths of the bands are (TM1 = 0.485 μm, TM2 = 0.560 μm, TM3 = 0.660 μm, TM4 = 0.830 μm TM5 = 1.650 μm and TM7 = 2.215 μm).

a very good separability between the compared spectra, whereas very low separability values (less than 1) indicate that the compared spectra might be appropriate to be combined into a single one. In the present study, spectral separability was performed by comparing the mean pixel spectral values of the selected training sites (essentially the mean digital numbers of at-sensor radiances). Their spectral separability was examined using both the first four channels of the Landsat TM (i.e. TM1, TM2, TM3 and TM4) and also all the sensor reflective channels, as SVM would be applied in both of these scenarios. Separability index for the training sites was found always higher than 1.18 and 1.58 for the case of a four- and six-band imagery, respectively, whereas for the validation points it was higher than 1.45 and 1.72, respectively. Also, at this point it is worthwhile to note that always lower separability was observed in the separation between the urban/industrial and the agricultural classes. This can also be observed in Fig. 3, which shows the mean spectra for each class versus all the reflective Landsat TM bands for the case of the selected set of training pixels.

4.2. SVM implementation

In the present study multiclass SVM pair-wise classification strategy was applied using ENVI image processing environment. This method is based on creating a binary classifier for each possible pair of classes, choosing the class that achieved the highest probability of identification across the series pair-wise comparisons. A number of studies have indicated that the kernel selection is important for the performance of the SVM classifier (Keuchel et al., 2003; Kavzoglu and Colkesen, 2009; Li and Liu, 2010), all the kernel functions available in ENVI software were applied in the present study. These are:

$$\text{Linear}: \quad K(x_i, x_j) = x_i^T x_j \tag{6}$$

$$\text{Polynomial}: \quad K(x_i, x_j) = (\gamma x_i^T x_j + r)^d, \quad \gamma > 0 \tag{7}$$

$$\text{Radial basis function}: \quad K(x_i, x_j) = \exp(-\gamma ||(x_i, x_j)||^2), \quad \gamma > 0 \tag{8}$$

$$\text{Sigmoid}: \quad K(x_i, x_j) = \tan H(\gamma x_i^T x_j + r) \tag{9}$$

where γ is the gamma term in the kernel function for all kernels except linear, d is the polynomial degree term in the kernel function of the polynomial kernel, r is the bias term in the kernel function for the polynomial and sigmoid kernels. γ, d, and r are user-defined parameters, as their correct definition significantly increases the SVM accuracy solution.

SVM was implemented in all cases at the original sensor spatial resolution (i.e. 30 m) for all different kernel types using initially the first four (TM1, TM2, TM3 and TM4) and subsequently using all the six reflective sensor spectral bands. This allowed examining the potential benefits of the inclusion of additional spectral information to both the SVM overall classification performance and also to the delineation of the total burnt area from the TM image. For the implementation of the different kernel functions a number of parameters needed to be set. Generally very little guidance exists in the literature concerning the criteria to be used in selecting the kernel-specific parameters (e.g. Carrao et al., 2008; Li and Liu, 2010). In the present study, parameterization of each of the four kernels was based on performing a number of trials of parameters combinations, using classification accuracy as a measure of quality, as has been previously implemented by other researchers (e.g. Pal and Mather, 2005; Kuemmerle et al., 2009). In addition, the kernel-parameter values given by other studies where SVM had been performed using TM data and the suggestions for the parameterization of these values for the different kernels given in the ENVI Software User's Guide (ENVE User's Guide, 2008) were also taken into account in parameterizing each kernel function. Common parameters which were set for all the selected kernels were the penalty parameter, the pyramid levels and the classification probability threshold value. The penalty parameter was set in all cases to its maximum value (i.e. 100), forcing all pixels in the training data to converge to a class. The pyramid parameter was set to a value of zero for all kernels, causing the Landsat TM image to be processed at full spatial resolution. A classification probability threshold of zero was also applied, restricting all image pixels to get exactly one class label, and no pixels to remain unclassified. For the γ parameter a value equal to the inverse of the number of the spectral bands of the Landsat TM imagery was specified each time (here equal to the value of 0.250 and 0.167 for the case of the selection of four and six spectral bands of Landsat TM, respectively). The bias in the kernel function required in the polynomial and sigmoid kernels was set in both cases equal to one, while in the polynomial kernel the degree of kernel polynomial was set equal to two.

4.3. Accuracy assessment

Classification accuracy was assessed based on the classification accuracy statistics, namely the error matrix (user/producer's accuracy and omission/commission error), overall accuracy and kappa statistic (Congalton and Green, 1999). Overall accuracy provides a measure of the overall accuracy of the classification and is expressed as percentage (%). The kappa statistic is a measure of the difference between the actual agreement between reference data and the classifier used to perform the classification versus the chance of agreement between the reference data and a random classifier. This parameter takes values between 0 and 1, where values greater than 0.80 represent generally a very good agreement between classification map and reference data. Producer's accuracy indicates the probability that the classifier has correctly labeled an image pixel whereas the user's accuracy expresses the probability that a pixel belongs to a given class and the classifier has labeled the pixel correctly into the same given class. Commission error (expressed as %) is derived by differentiating the user's accuracy (also expressed as %) from 100, whereas the omission error (%) is computed by differentiating the producer's accuracy (%) from 100. In the present study, validation of the classification maps produced from the SVM implementation was performed against the set of validation pixels for each class collected following the procedure described earlier in the pre-processing phase (see Section 4.1). In addition to the classification statistics, the SVM-derived burnt

area estimate was also compared against the Risk-EOS burnt area estimate which had been acquired. Analogous studies performing comparisons of different burnt area estimation methods versus Risk-EOS estimates have been available in the past by Zammit et al. (2006) and recently by Kontoes et al. (2009).

5. Results and discussion

5.1. SVM overall classification performance

SVM classification of the post-fire Landsat TM scene resulted in the generation of the thematic maps of land use/land cover shown in Fig. 4 in which the burnt area class is depicted in red. The results obtained for the different classification experiments shown in Fig. 4 are summarised in Table 1. Generally classification of the Landsat TM data with the SVM using either the first four (i.e. TM1, TM2, TM3 and TM4) or all the reflective bands of the image, provided good results for each kernel function used in terms of the overall accuracy and kappa statistic. Both overall accuracy and kappa statistic were always higher than 93% and 0.920, respectively for all thematic maps produced. User's and producer's accuracy of the individual classes was also generally very high for all classifications, in all cases higher than 79 and 81%, respectively. In terms of the individual land cover classes results, user's and producer's accuracies obtained (Table 1) showed a clear separation of the forest, and burnt area classes in all classification scenarios performed, whereas for the linear kernel in particular, clearly separable was also the urban fabric/bare soil class. The scrubland/herbaceous vegetation and the agricultural areas classes generally exhibited the lowest classification accuracy in all classification scenarios. However, even for those two classes, high enough and fully acceptable from an operational point of view application as the classification accuracy achieved ranges from 82 to 95%. The lower classification accuracy of the scrubland/herbaceous vegetation and the agricultural areas classes could be probably related to the generally low spectral separability of those two classes in the TM imagery. This was evidenced in all the separability index computation performed during the selection of the training and validation points, for both when the four and six TM spectral bands were considered (see Section 4.1 and Fig. 2). Use of all the reflective Landsat TM channels in the SVM implementation also improved the separation of the urban/industrial areas class in all kernels used. Nevertheless, training points selection was not influential to the classification results obtained, as if this was the case then the confusion matrix produced would not allow obtaining such high user's and producer's accuracies for each class.

As regards the effect of kernel function selection to the SVM classification applied to the TM imagery, results generally showed small differences in the overall classification. Both when only the four and all sensor bands are employed in the SVM classification, the linear and polynomial kernels are producing somewhat higher classification accuracy, in comparison to the RBF and the sigmoid kernels. If only the four TM bands are used in the classification, then the RBF is producing generally equally good results to those of the linear kernel, whereas in the case where all the reflective TM bands are used in classification, the polynomial kernel is producing after the linear the higher classification results from all kernels compared herein. Zhu and Blumberg (2002) using ASTER imagery acquired for a site in Israel reported generally very close results in the SVM classification accuracy when either the polynomial or the RBF kernel was used in classification. Results obtained herein are generally in agreement with Dixon and Candade (2008), who examined the use of different kernel functions selection to the SVM classification performance using also TM data acquired for a site in Florida, USA, and reported the linear and polynomial kernels to produce high overall classification accuracy and kappa statistic in comparison to RBF kernel.

Use of different number of TM spectral bands in the SVM classification showed negligible differences in the overall classification accuracies obtained for the different kernel functions used. At least for this specific cases study, use of all the reflective TM bands somehow slightly improved the overall classification performance of the SVM when the linear and the polynomial kernel functions are used, whereas the opposite happened when the RBF and sigmoid functions are used. At this point it is worthwhile to note that, in analogous study Pal and Mather (2005) using Landsat ETM+ data and RBF kernel function reported an increase in the SVM classification accuracy as the number of features (bands) increased, which is in agreement with the results of the present study at least for the results obtained from the linear and polynomial kernels. However, in another study, Dalponte et al. (2009), using airborne hyperspectral observations examined the influence of spectral resolution to the SVM classification performance for two test regions in Italy and reported a modest effect of number of spectral bands in the classification kappa coefficient.

All in all, classification accuracies reported here are of similar, or sometimes better, to those reported by other studies investigating the combined use of SVM classifier with TM imagery or with other types of remote sensing data in a Mediterranean setting or dissimilar ecosystems (e.g. Carrao et al., 2008; Yang et al., 2008; Huang et al., 2008; Knorn et al., 2009; Kavzoglu and Colkesen, 2009; Otukei and Blaschke, 2010; Dalponte et al., 2009). Classification accuracy results reported herein are also of similar accuracy compared to other studies deriving burnt area estimates from Landsat TM based on other classification approaches using similar number of classes in their classification (e.g. Sunar and Ozkan, 2001; Hudak and Brockett, 2004; Quintano et al., 2006). Petropoulos et al. (2010) investigated the potential value of Artificial Neural Networks (ANN) and Spectral Angle Mapper (SAM) classifiers combined with TM imagery for burnt area mapping for the same to here study region. Authors reported an overall accuracy and kappa statistic of 90.29% and 0.878 and of 83.82% and 0.795 in the ANN and SAM classifiers implementation, respectively, which is lower to those obtained here, suggesting that SVM can generally produce more accurate classification when is combined with TM imagery.

Generally, the high accuracies obtained in the separability of the different classes, including the burnt area, can be attributed partly to the differences in the spectral properties between the other classes and that of the burnt area, which were even more evidenced in the Landsat TM middle infrared bands TM5 and TM7. These bands are generally sensitive to discriminating vegetation at varying moisture levels and burnt areas which were completely open and had very low moisture levels. Also, it should be noted that the imagery used in the present study was acquired during the dry season, which is when the differences between the vegetation at different moisture content conditions and bare soil are discriminated.

5.2. Burnt area delineation from SVM

Table 2 is summarising the total burnt area estimates and their differences between the different classifications performed for the same geographical area for which was available the burnt area estimate from Risk-EOS. In addition, Fig. 5 depicts the spatial agreement in the burnt area estimates between the Risk-EOS and the SVM-based each time estimate for the different SVM implementations performed herein. As regards the total burnt area estimate, results showed moderate differences in its estimation by the classification scenarios implemented, with an absolute difference ranging from 0.20 to 0.90 km^2 in comparison to the burnt area estimate reported by Risk-EOS. Total burnt area estimate produced

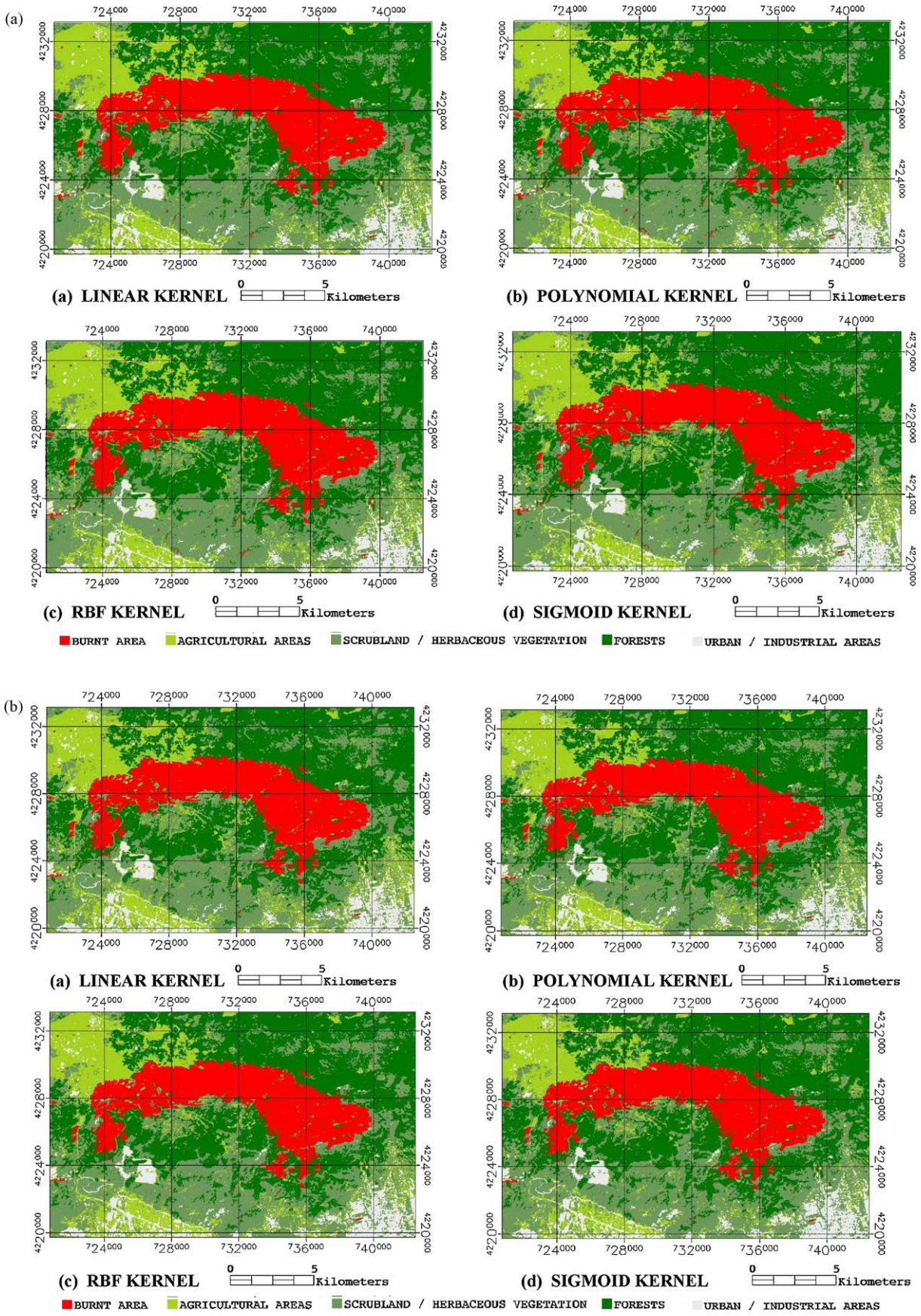

Fig. 4. (a) Thematic maps from the SVM classifier implementation to the TM imagery using only the first four sensor's spectral bands (b) Thematic maps from the SVM classifier implementation to the TM imagery using all the sensor's spectral bands.

Table 1
Classification results obtained from the SVM implementation with the Landsat TM imagery for the different combinations of kernel functions and sensor's spectral bands.

	4 spectral channels of Landsat TM used							
Kernel type	Linear		Polynomial		RBF		Sigmoid	
Land cover classes	Producer's accuracy (%)	User's accuracy (%)	Producer's accuracy (%)	User's accuracy (%)	Producer's accuracy (%)	User's accuracy (%)	Producer's accuracy (%)	User's accuracy (%)
Agricultural areas	84.75	92.59	84.75	92.59	84.75	92.59	83.05	90.74
Forests	100	100	100	100	100	100	100	100
Scrubland/herbaceous vegetation	94.12	85.71	94.12	85.71	94.12	85.71	90.20	83.64
Urban fabric/bare soil areas	98.08	98.08	98.08	98.08	98.08	98.08	100	98.11
Burnt area	100	100	100	100	100	100	100	100
Overall accuracy	95.89		95.87		95.89		95.87	
Kappa coefficient	0.948		0.948		0.948		0.948	
	6 spectral channels of Landsat TM used							
Kernel type	Linear		Polynomial		RBF		Sigmoid	
Land cover classes	Producer's accuracy (%)	User's accuracy (%)	Producer's accuracy (%)	User's accuracy (%)	Producer's accuracy (%)	User's accuracy (%)	Producer's accuracy (%)	User's accuracy (%)
Agricultural areas	86.44	94.44	84.75	92.59	84.75	92.59	81.36	84.21
Forests	100	100	100	100	100	100	100	100
Scrubland/herbaceous vegetation	94.12	85.71	92.16	83.93	92.16	83.93	82.35	79.25
Urban fabric/bare soil areas	100	100	100	100	100	100	100	100
Burnt area	100	100	100	100	100	100	100	100
Overall accuracy	96.51		95.89		95.87		93.67	
Kappa coefficient	0.956		0.948		0.948		0.920	

from the different SVM classifier scenarios was always lower in comparison to that reported by Risk-EOS. Higher differences in total burnt area estimates found in most cases when all the reflective spectral bands of the sensor were employed in the SVM classification scheme in comparison to when only the first four spectral bands (i.e. TM1, TM2, TM3 and TM4) were used. The total burnt area estimate from the SVM implementation closer to that from Risk-EOS was that from the implementation of the SVM classifier using the polynomial kernel using the four only reflective bands of the Landsat TM imagery (difference of 0.20 km^2 or 0.42% from Risk-EOS). The next closer burnt area estimate to that of Risk-EOS was that of the SVM classifier applied using the RBF kernel and also the first four reflective TM bands (difference of 0.23 km^2 or 0.48% from Risk-EOS). When all reflective sensor bands were included in the SVM classification, the closer total burnt area estimate to that reported by Risk-EOS was when the linear kernel was used (difference of 0.32 km^2 or 0.68% from Risk-EOS).

Clearly, the burn scar area shape was also generally similar between the different classifications (Fig. 5) and also with that reported by Risk-EOS, suggesting a generally good spatial agreement between the compared datasets. As clearly illustrated in Fig. 5, differences in the burnt area estimates were found mainly in all cases mainly in the north and south parts of the burn scar and also in some specific regions inside the perimeter of the burn scar. As seen from Fig. 5, areas identified as burnt by Risk-EOS in the south part and inside the burnt scar envelope have been omitted by SVM in all scenarios, thus correspond to representing omission errors by SVM classification. Similarly, in the north part of the burnt area areas have been falsely identified by SVM as burnt areas, representing commission errors of the SVM burnt area classification. A visual inspection of these misclassifications with the originally acquired TM imagery and also with the CORINE 2000 land nomenclature map indicated that most of the omission errors observed in the south region and inside the area of the burn scar envelope are associated with different types of forested area, whereas the commission errors observed in the north region mainly with agricultural areas that covered this region. Results obtained at least for this specific case study, also generally indicate that selection of any combination of spectral bands and the kernel function has a generally modest impact to the delineation of the burnt area estimate from the Landsat TM imagery. This is in agreement to the findings from the overall classification accuracy assessment performed earlier (Section 5.1).

Differences in the burnt area mapped may be related to the responses of different land cover/use types during the fire evolution and also after the fire suppression, which might be related also to the degree of biomass burning severity from the fire passing (e.g. Smith et al., 2007). For example, surface fires over forested regions generally burn totally the understory and do not burn the top of the forest trees canopy due to the speed by which those are progressing, and as a result those regions are not identified as burnt in satellite imagery (omission errors). What is more, misclassification errors of land surface cover types having similar spectral characteristics as

Table 2
Total burnt area estimate from the SVM implementation with the Landsat TM imagery for the different combinations of kernel functions and sensor's spectral bands. The total burnt area estimate obtained from the Risk-EOS service is also reported.

Kernel type	4 Spectral bands of Landsat TM Total burnt area (km^2)	Absolute difference from Risk-EOS (km^2)	6 Spectral bands of Landsat TM Total burnt area (km^2)	Absolute difference from Risk-EOS (km^2)
Linear	46.86	0.60	46.94	0.32
Polynomial	47.06	0.20	46.63	0.63
RBF	47.03	0.23	46.66	0.94
Sigmoid	46.81	0.45	46.40	0.86
RISK-EOS total burnt area estimate	47.26		47.26	

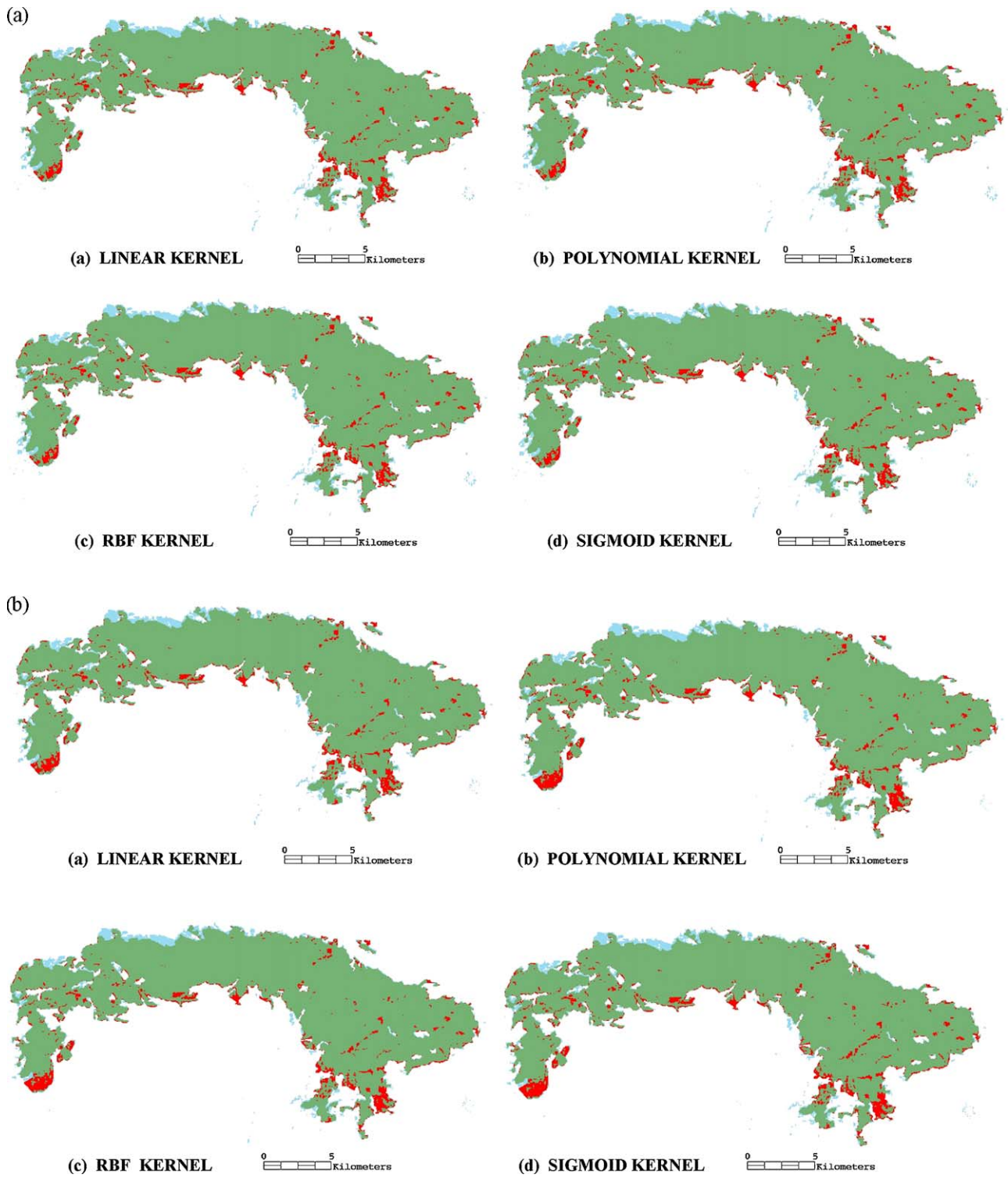

Fig. 5. (a) Comparisons of the results from the various kernels using the different number of spectral bands of the Landsat TM imagery. With the blue is the area identified as burnt only from the SVM classifier using the first four bands of the TM imagery, with red the burnt area estimated from Risk-EOS which was not identified as burnt from SVM implementations, whereas with green the commonly identified burnt area between the SVM scenarios implementation and Risk-EOS. (b) Comparisons of the results from the various kernels using the different number of spectral bands of the Landsat TM imagery. With the blue is the area identified as burnt only from the SVM classifier using all the reflective bands of the TM imagery, with red the burnt area estimated from Risk-EOS which was not identified as burnt from SVM implementations, whereas with green the commonly identified burnt area between the SVM scenarios implementation and Risk-EOS. (For interpretation of the references to color in this figure legend, the reader is referred to the web version of the article.)

burnt areas, even so given the high degree of vegetation fragmentation and heterogeneity that exists in Mediterranean ecosystems, such as that used in the present study. For example shaded areas have generally shown to have similar spectral signatures to those of burnt areas (Tanaka et al., 1983; Pereira et al., 1997). Last but not least, differences in the total burnt area estimates can be attributed to the differences in the spatial resolution between the burnt area maps produced from the TM sensor (at 30 m spatial resolution)

and the reference burnt area estimate which had based on SPOT XS imagery analysis (20 m spatial resolution), which can be even more significant in regions with high degree of vegetation fragmentation.

Results from the present study are also comparable in terms of the burnt area detection to other studies carried out previously but with different types of satellite datasets. Zammit et al. (2006) applied a binary (burnt/sunburnt) SVM classification using SPOT5 multispectral imagery acquired for a site in southern France and their validation against Risk-EOS observations indicated generally overall classification accuracy higher than 98%. In a similar study, Cao et al. (2009), also applied a binary SVM classification scheme for burnt area retrieval from MODIS Terra imagery and validations which they performed for a test site between Mogolia and China versus burnt area estimates acquired from TM imagery, showed an overall accuracy of 96.8% and a kappa statistic of 0.933. Petropoulos et al. (2010), recently for the same test site used in the present study evaluated the combined use of TM imagery with ANN and SAM classifiers and reported absolute differences from the Risk-EOS of 0.52 km^2 (or equivalently 1.1%) and 2.38 km^2 (or equivalently 5%) for the ANN and SAM, respectively. In comparison to their results, results obtained in the present study using the SVM classifier were of closer agreement to the Risk-EOS estimate, suggesting that SVM, at least for this specific case, performs better than ANN or SAM classifier when combined with TM imagery. All in all, burnt area estimated from the combined use of SVM with the TM imagery generally produced very close estimates to those of Risk-EOS, both in terms of absolute total burnt area values and of the spatial agreement of the burnt area cartography. This is a very important finding from an operational point of view of using the SVM classifier in burnt area mapping, given that the Risk-EOS estimates had been based in the analysis of higher spatial resolution SPOT5 imagery assisted by very high resolution IKONOS imagery photo-interpretation and field visits performed in the studied region.

6. Conclusions

The present study was concerned with the evaluation of the potential of combined use of SVM classifier with Landsat TM imagery for obtaining burnt area mapping in a Mediterranean setting.

Evaluation of the performance of the SVM classifier in delineating burnt areas on a Landsat TM scene for this specific fire event was based on standard classification accuracy assessment metrics (Congalton and Green, 1999). Additional comparisons of the derived burnt area maps were also performed against the Risk-EOS operational service estimate corresponding to this specific fire, derived from the implementation of an NDVI-threshold algorithm to SPOT4 XS (20 m spatial resolution) imagery combined with very high spatial resolution IKONOS photo-interpretation refinement applied at a post-classification stage. Implementation of the SVM using different kernel functions as well as spectral band combinations of Landsat TM imagery acquired very shortly after the fire suppression showed a high overall classification performance. Overall classification accuracy ranged from 93 to 96% and a kappa coefficient varied from 0.920 to 0.956, respectively. Overall, these results were in agreement with other studies in which the SVM classifier has been combined with Landsat TM/ETM+ in various, not burnt area mapping-specific classification problems (Kavzoglu and Colkesen, 2009) or with other works investigating the retrieval of burnt area estimates from Landsat TM (Quintano et al., 2006). Analysis of the effects of the number of spectral bands and of the different kernel functions on the SVM-based classification accuracy indicated, at least for the present study, no significant change to the overall classification accuracy. However, an improvement in the agreement between the Risk-EOS total burnt area estimate and that derived from the implementation of the different kernels was observed when all the Landsat TM bands were employed in the SVM only when the linear kernel was used.

Although this study has been restricted to illustrating the ability of Landsat TM sensor in burnt area mapping of a single fire event, the results confirmed the potential of the SVM classifier combined with Landsat TM satellite imagery for performing rapid and cost-effective fire analysis of regional scale (~1:50,000) fire episodes to other Mediterranean like ecosystems. Furthermore, results from the present work may have practical applications from the point of view of the use of the 30 m spatial resolution of the freely distributed Landsat TM imagery coupled with the unique properties of SVM classifier for supporting, and even complementing, existing burnt area monitoring methods operated by civil protection and other agencies (e.g. Risk-EOS, EFFIS), providing "validated" relevant observations, often in the form of regional-scale products. What is more, the SVM-based classification provided high classification results in overall, evidencing the potential of the method for an all-inclusive land use/land cover mapping. Results from this study also suggested that even in a complex classification scheme, SVM classifier can delineate accurately the burnt area, providing results of burnt area that are not minimally based in creating masks of burnt/non-burnt area, as is the norm by other studies performed previously (Zammit et al., 2006; Cao et al., 2009; Kontoes et al., 2009). This is also important, as it indicates an encouraging potential of the SVM method to be adopted towards other classification-based applications.

Nevertheless, from an operational view angle, requirements of the method in computing resources and computational time were also very reasonable. However, the computational time in SVM implementation when dealing with large datasets in terms of area covered, and spectral and spatial resolution should be further investigated in the future as part of the examination of the full potential of this technique for operational application. Also, from an operational perspective again, although the present results show a very promising potential for using SVM in burnt area mapping, surely further research is required towards the extension of the direction of the investigation of the parameters creating the largest uncertainty in the estimation of burnt area and of the SVM classification accuracy in overall. An important direction of future work includes a detailed investigation of the effect of different kernels parameterization and at different implementation conditions. Furthermore, a systematic research on the effect of additional spectral information that can be derived from the original data (such as of the principal analysis components, the NDVI, NBR or texture bands created based on spectral variances), which can perhaps assist in increasing further the SVM overall classification performance, as well as the detection of burnt areas from remote sensing data.

Acknowledgements

Authors gratefully acknowledge the United Stated Geological Survey (USGS) for providing free access to Landsat TM satellite imagery worldwide. In addition authors are thankful to the anonymous reviewers for their useful feedback which resulted to the overall improvement of the originally submitted manuscript.

References

Bochetti, L., Roy, D., Barbosa, P., Boca, R., Justice, C.A., 2008. A MODIS assessment of the summer 2007 extent burnt in Greece. International Journal of Remote Sensing 29 (8), 2433–2436.

Burges, C., 1998. A tutorial on support vector machines for pattern recognition. Data Mining and Knowledge Discovery 2 (2), 121–167.

Cao, X., Chen, J., Matsushita, B., Imura, H., Wang, L., 2009. An automatic method for burn scar mapping using support vector machines. International Journal of Remote Sensing 30 (3), 577–594.

Carrao, H., Goncalves, P., Caetano, M., 2008. Contribution of multispectral and multitemporal information from MODIS images to land cover classification. Remote Sensing of Environment 112, 986–997.
Congalton, R., Green, K., 1999. Assessing the Accuracy of Remotely Sensed Data: Principles and Practices. CRC/Lewis Press, Boca Raton, FL, 137 pp.
Corona, P., Lamonaca, A., Chirici, G., 2008. Remote sensing support for post fire forest management. iForest 1, 6–12 (accessed 28.02.08) http://www.sisef.it/iforest/.
Cuomo, V., Lasaponara, R., Tramutoli, V., 2001. Evaluation of a new satellite-based method for forest fire detection. International Journal of Remote Sensing 22 (9), 1799–1826.
Dalponte, M., Bruzzone, L., Vescovo, L., Gianelle, D., 2009. The role of spectral resolution and classifiers complexity in the analysis of hyperspectral images of forest areas. Remote Sensing of Environment 113, 2345–2355.
Deering, D.J., Rouse, J.W., Haas, R.H., Schell, J.A., 1975. Measuring production of grazing units from Landsat MSS data. In: Proceedings of the 10th International Symposium of remote Sensing of Environment, ERIM, Ann Arbor, Michighan, August 23–25, pp. 1169–1178.
Dixon, B., Candade, N., 2008. Multispectral land use classification using neural networks and support vector machines: one or the other, or both? International Journal of Remote Sensing 29 (4), 1185–1206.
Eckmann, T.C., Roberts, D.A., Still, C., 2008. Using multiple endmember spectral mixture analysis to retrieve subpixel fire properties from MODIS. Remote Sensing of Environment 112, 3773–3783.
ENVI User's Guide, 2008. ENVI On-line Software User's Manual, ITT Visual Information Solutions.
Escuin, S., Navarro, R., Fernández, P., 2008. Fire severity assessment by using NBR (Normalised Burn ratio) and NDVI (Normalised Difference Vegetation Index) derived from LANDSAT TM/ETM images. International Journal of Remote Sensing 29 (4), 1053–1073.
European Commission, Forest Fires in Europe, 2006. Joint Research Centre, Institute for Environment and Sustainability, Report No. 7, EUR 22931 EN, Luxembourg, Office for Official Publications of the European Communities, 78 pp, ISSN:1018-5593.
Eva, H., Lambin, E.F., 2000. Fires and land-cover change in the tropics: a remote sensing analysis at the landscape scale. Journal of Biogeography 27, 765–776.
FAO, 2001. Global forest fire assessment 1990–2000, 2001. Forest Resources Assessment Programme, Working Paper No. 55, http://www.fao.org/forestry/fo/fra/docs/Wp55_eng.pdf (accessed 14.04.09).
Foody, G.M., Mathur, A., 2004. A relative evaluation of multiclass image classification by support vector machines. IEEE Transactions on Geosciences and Remote Sensing 42, 1335–1343.
Giglio, L., Csiszar, I., Justice, C.O., 2006. Global distribution and seasonality of active fires as observed with the Terra and Aqua MODIS sensors. Journal of Geophysical Research—Biogeosciences 111, G02016.
Huang, C., Davis, L.S., Townshend, J.R.G., 2002. An assessment of support vector machines for land cover classification. International Journal of Remote Sensing 23, 725–749.
Huang, C., Song, K., Kim, S., Townshend, J.R.G., Davis, P., Masek, J.G., Goward, S.N., 2008. Use of dark object concept and support vector machines to automate forest cover change analysis. Remote Sensing of Environment 112, 970–985.
Hudak, A.T., Brockett, B.H., 2004. Mapping fire scars in a southern African savanna using Landsat imagery. International Journal of Remote Sensing 25 (16), 3231–3243.
Jayaweera, I., Ahlnas, I., 1974. Detection of thunderstorms from satellite imagery for forest fire control. Journal of Forestry, 767–770.
JRC-EEA, 2005. CORINE land cover updating for the year 2000: Image 2000 and CLC2000. In: Lima, V. (Ed.), Products and Methods. Report EUR 21757 EN. JRC-Ispra (accessed 28.11.09).
Kasischke, E.F., French, N.H.F., 1995. Locating and estimating the aerial extent of wildfires in Alaskan boreal forests using multiple-season AVHRR NDVI composite data. Remote Sensing of Environment 51, 263–275.
Kavzoglu, T., Colkesen, I., 2009. A kernel functions analysis for support vector machines for land cover classification. International Journal of Applied Earth Observation and Geoinformation 11, 352–359.
Keuchel, J.S., Naumann, M., Heiler, A., Siegmund, 2003. Automatic land cover analysis for Tenerife by supervised classification using remotely sensed data. Remote Sensing of Environment 86, 53–541.
Knorn, J., Rabe, A., Radeloff, V.C., Kuemmerle, T., Kozak, J., Hostert, P., 2009. Land cover mapping of large areas using chain classification of neighbouring Landsat satellite images. Remote Sensing of Environment 113, 957–964.
Kokaly, R.F., Rockwell, B.W., Haire, S.L., King, T., 2007. Characterisation of post-fire surface cover, soils and burn severity at the Cerro Grande Fire, New Mexico, using hyperspectral and multispectral remote sensing. Remote Sensing of Environment 106, 305–325.
Kontoes, C.C., Poilve, H., Florsch, G., Keramitsoglou, I., Paralikidis, S., 2009. A comparative analysis of a fixed thresholding vs. a classification treeapproach for operational burn scar detection and mapping. International Journal of Applied Earth Observation and Geoinformation 11, 299–316.
Koutsias, N., Karteris, M., Fernandez-Palacios, A., Navarro, C., Jurado, J., Navarro, R., Lobo, A., 1999. Burned land mapping at local scale. In: Chuvieco, E. (Ed.), Remote Sensing of Large Wildfires in the European Mediterranean Basin. Springer-Verlag, Berlin, Heidelberg, pp. 157–187.
Kuemmerle, T., Chaskovskyy, O., Knorn, J., Radeloff, V.C., Kruhlov, I., 2009. Forest cover change and illiegal logging in the Ukranian Carpathians in the transition period from 1988 to 2007. Remote Sensing of Environment 113, 1194–1207.
Lentile, L.Z., Holden, A., Smith, A.M.S., Falkowski, A.M.J., Hudak, A.T., Morgan, P., Lewis, Sarah A., Gessler, P.E., Benson, N.C., 2006. Remote sensing techniques to assess active fire characteristics and post-fire effects. International Journal of Wildland Fire 15, 319–345.
Li, D.-C., Liu, C.-W., 2010. A class possibility based kernel to increase classification accuracy for small data sets using support vector machines. Expert Systems with Applications 37, 3104–3110.
Maselli, F., Romanelli, S., Bottai, L., Zipoli, G., 2003. Use of NOAA-AVHHR NDVIK images for the estimation of dynamic fire risk in Mediterranean areas. Remote Sensing of Environment 86, 187–197.
Mather, P.M., 2004. Computer-Processing of Remotely-sensed Images, third Ed. John Wiley and Sons, Chichester.
Mayor, A.G., Bautista, S., Lovet, J., Bellot, J., 2007. Post-fire hydrological and erosional responses of a Mediterranean landscape: seven years of catchment-scale dynamics. Catena 71, 68–75.
Naveh, Z., 1975. The evolutionary significance of fire in the Mediterranean region. Vegetation 29 (3), 199–208.
Otukei, J.R., Blaschke, T., 2010. Land cover change assessment using decision trees, support vector machines and maximum likelihood classification algorithms. International Journal of Applied Earth Observation and Geoinformation 12S, S27–S31.
Pal, M., Mather, P.M., 2005. Support Vector Machines for classification in remote sensing. International Journal of Remote Sensing 26 (5), 1007–1011.
Pal, M., 2006. Support vector machine-based feature selection for land cover classification: a case study with DAIS hyperspectral data. International Journal of Remote Sensing 27 (14), 2877–2894.
Pal, M., Mather, P.M., 2006. Some issues in the classification of DAIS hyperspectral data. International Journal of Remote Sensing 27, 2895–2916.
Pereira, J.M.C., Chuvieco, E., Beudoin, A., Desbois, N., 1997. Remote sensing of burned areas: a review. In: Chuvieco, E. (Ed.), A Review of Remote Sensing Methods for the Study of Large Wildland Fires. Departamento de Geografiïa, Universidad de Alcalaï, Alcalaï de Henares, pp. 127–184.
Petropoulos, G., Vadrevu, K.P., Xanthopoulos, G., Karantounias, G., Scholze, M., 2010. A comparative analysis of spectral angle mapper and artificial neural network classifiers for obtaining burnt area cartography from Landsat TM data. Sensors 10, 1967–1985.
Piper, J., 1992. Variability and bias in experimentally measured classifier error rates. Pattern Recognition Letters 13, 685–692.
Quintano, C., Fernandez-Manso, A., Fernandez-Manso, O., Shimabukuro, Y.E., 2006. Mapping burnt areas in Mediterranean countries using spectral mixture analysis from a uni-temporal perspective. International Journal of Remote Sensing 27 (4), 645–662.
Rong, R.L., Kaufman, J., Hao, W.M., Salmon, J.M., Gao, B.-C., 2004. A technique for detecting burn scars using MODIS data. IEEE Transactions on Geoscience and Remote Sensing 42 (6), 1300–1308.
Rosa, De La J.M., Gonzalez-Perez, J.A., Gonzalez-Vazquez, R., Knicer, H., Lopez-Capel, E., Manning, D.A.C., Gonzalez-Vila, F.J., 2008. Use of pyrolisis/GC-MS combined with thermal analysis to monitor C and N changes in soil organic matter from a Mediterranean fire affected forest. Catena 74, 296–303.
Simard, M., Saatchi, S.S., De-Grandi, G., 2000. The use of decision tree and multiscale texture for classification of JERS-1 SAR data over Tropical forest. IEEE Transactions on Geoscience and Remote Sensing 38 (5), 2310–2321.
Smith, A.M.S., Drake, N.A., Wooster, M.J., Hudak, A.T., Holden, Z.A., Gibbons, C.J., 2007. Production of Landsat ETM+ reference imagery of burnt areas within Southern African savannahs: comparison of methods and application to MODIS. International Journal of Remote Sensing 28 (12), 2753–2775.
Sunar, F., Ozkan, C., 2001. Forest fire analysis with remote sensing data. International Journal of Remote Sensing 22 (12), 2265–2277.
Tanaka, S., Kimura, H., Suga, Y., 1983. Preparation of a 1: 25 000 Landsat map for assessment of burnt area on Etajima Island. International Journal of Remote Sensing 4, 17–31.
Van Niel, T.G., McVicar, T.R., Datt, B., 2005. On the relationship between training sample size and data dimensionality of broadband multi-temporal classification. Remote Sensing of Environment 98, 468–480.
Vapnik, V., 1995. The Nature of Statistical Learning Theory. Springer-Verlag, New York, NY.
Verbyla, D.L., Boles, S.H., 2000. Bias in land cover change estimates due to misregistration. International Journal of Remote Sensing 21, 3553–3560.
Yang, Q., Li, X., Shi, X., 2008. Cellular automata for simulating land use changes based on support vector machines. Computers and Geosciences 34, 592–602.
Zammit, O., Descombes, X., Zerubia, J., 2006. Burnt area mapping using Support Vector Machines. Forest Ecology and Management, 234–240.
Zhu, G., Blumberg, D.G., 2002. Classification using ASTER data and SVM algorithms. The case study of Beer Sheva, Israel. Remote Sensing of Environment 80, 233–240.